Journal of Molecular Structure 1148 (2017) 111–118

Contents lists available at ScienceDirect

Journal of Molecular Structure

journal homepage: http://www.elsevier.com/locate/molstruc

Structural and spectroscopic characterization of the second polymorph of 1-methylhydantoin

Bernardo A. Nogueira [a, *], Gülce O. Ildiz [a, b], Marta S.C. Henriques [c], José António Paixão [c], Rui Fausto [a]

[a] CQC, Department of Chemistry, University of Coimbra, Portugal
[b] Faculty of Sciences and Letters, Department of Physics, Istanbul Kültür University, Ataköy Campus, Bakırköy, Istanbul 34156, Turkey
[c] CFisUC, Department of Physics, University of Coimbra, Portugal

ARTICLE INFO

Article history:
Received 19 June 2017
Accepted 12 July 2017
Available online 13 July 2017

Keywords:
1-Methylhydantoin
Polymorphism
Raman spectroscopy
X-ray diffraction

ABSTRACT

In a previous study [Nogueira, B. A.; Ildiz, G. O.; Canotilho, J.; Eusébio, M. E. S.; Fausto, R. *J. Phys. Chem. A*, **2014**, *118*, 5994–6008], two different polymorphs of 1-methylhydantoin (1-MH, $C_4H_6N_2O_2$) were identified using infrared spectroscopy, differential scanning calorimetry and polarized-light thermal microscopy. Unfortunately, at that time it was not possible to structurally characterize in detail the second polymorph (polymorph II) of the compound, due to lack of suitable crystals for X-ray diffraction structure determination. In this article, a throughout investigation of the polymorphism of 1-MH is presented. Screening for polymorphs was performed by recrystallization from different solvents, and the structure of polymorph II was determined for the first time by single crystal X-ray diffraction. The spectroscopic characterization of this polymorph was also undertaken, by Raman spectroscopy, which was also used to follow the phase transition between the two polymorphs (the well-known polymorph I, and the newly described polymorph II), showing that even though their structures are significantly distinct, the transition is a non-destructive one.

1. Introduction

1-methylhydantoin (1-MH; Scheme 1) belongs to the hydantoin family of compounds, which are heterocycles that derive from imadazolidine, bearing two carbonyl groups at the C2 and C4 positions. Substituents can be present at the remaining atoms of the ring (C5, N1 or N3). In the case of 1-MH, a single methyl substituent is attached to N1.

The physiological activity of hydantoins is well known, namely as anticonvulsive, anti-inflammatory, antiepileptic and anticancer drugs [1–6]. The use of some substituted hydantoins for the treatment of HIV-1 has also been suggested [7,8].

Recently, we have reported on the molecular structure, infrared spectra (in different environments, including under matrix isolation conditions), photochemistry and thermal properties of 1-MH [9]. In the neat solid phase, the compound was characterized in a polymorphic variety named polymorph I, whose crystalline structure had already been determined previously by Puszyńska-Tuszkanow and co-workers [10]. In our study [9], a second polymorph of the compound (polymorph II) was obtained by sublimation of polymorph I at $T = 100$ °C and $p = 103$ Pa using the cold finger technique, with water at ~20 °C as the freezing fluid. However, the structure of this crystalline variety could not be obtained, since the gathered crystals were of insufficient quality for X-ray structure determination.

Nevertheless, some clues regarding the structure of polymorph II were extracted from the obtained infrared data [9]. In particular, by considering the relative values of the frequency shifts of the bands associated with the NH stretching and rocking modes (ν(NH) and γ(NH)) to lower and higher values, respectively, in relation to their position in the IR spectrum obtained for the isolated 1-MH molecule in an argon matrix, it was possible to conclude that polymorph II should have a globally slightly weaker H-bond network than polymorph I [9].

The aim of the present study was to undertake a more complete investigation of the polymorphism exhibited by 1-methylhydantoin. Screening for polymorphs was made by characterizing samples resulting from recrystallization in different

* Corresponding author.
E-mail address: ban@qui.uc.pt (B.A. Nogueira).

http://dx.doi.org/10.1016/j.molstruc.2017.07.028
0022-2860/

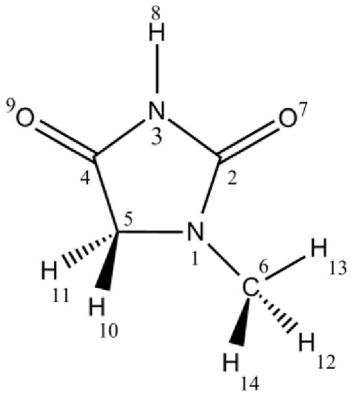

Scheme 1. 1-Methylhydantoin molecule, with atom numbering.

solvents, using Raman spectroscopy as the main probing technique. Polymorph II was successfully produced as the sole form from recrystallization in methanol, which yielded single crystals of enough good quality to be used for X-ray structure determination. The newly structurally described 1-MH polymorph II was then characterized by Raman spectroscopy. Besides, temperature variation single crystal Raman studies allowed to follow the transition between the two polymorphs (I and II).

2. Experimental

2.1. Crystal growth and screening

A commercial sample of 1-methlyhydantoin was obtained from Sigma-Aldrich (98% purity). The crystal screening considered samples of the compound obtained from recrystallization in different solvents, achieved by room temperature slow evaporation of the solvent. Two polymorphs were obtained: the previously characterized structurally polymorph I [9,10] was obtained upon recrystallization from dichloromethane, dioxane, water and ethanol solutions; polymorph II was obtained upon recrystallization from methanol. Recrystallizations from acetone and tetrahydrofurane (THF) solutions gave rise to a mixture of both polymorphs, although polymorph I appears most of times as the major constituent in both cases. The characterization of the samples was performed as described below.

2.2. Raman measurements

Macro Raman spectra were collected using a Nicolet DXR SmartRaman spectrometer, with 780 nm excitation source (frequency-stabilized single mode diode laser) and 5 cm^{-1} spectral resolution. Single crystal Raman spectra were obtained using a Horiba LabRam HR Evolution spectrometer, equipped with a Synapse CCD detector, a high-stability BXFM confocal microscope and a 600 gr mm^{-1} grating, with 633 nm HeNe laser excitation. In all

Table 1
Crystallographic parameters for the two polymorphs of 1-MH.[a]

Unit cell dimensions	Polymorph I [10]	Polymorph II
a (Å)	5.601(10)	19.0258(4)
b (Å)	12.178(3)	3.91210(10)
c (Å)	8.090(2)	6.82880(10)
α (°)	90	90
β (°)	105.62(2)	90
γ (°)	90	90
Volume (Å^3)	531.4(2)	508.273(18)
Space Group	$P2_1/c$	$Pna2_1$
Z	4	4
D_{calc} (g cm^{-3})	1.426	1.491
Absorption coefficient (mm^{-1})	0.116	0.121
F (0 0 0)	240	240

[a] Uncertainties, in parentheses, in units of the last digit.

Table 2
Hydrogen bond parameters for the two polymorphs of 1-MH.[a]

Hydrogen bond D-H··A	Distance D-H (Å)	Distance H ··· A (Å)	Distance DA (Å)	Angle DHA (°)
Polymorph I [10]				
N3—H8··O7	0.93(2)	1.888(19)	2.8148(17)	173.5(16)
C5—H10··O7	0.973(18)	2.598(19)	3.455(2)	147.2(13)
Polymorph II				
N3—H8··O7	0.81(3)	2.01(3)	2.816(2)	173(3)
C5—H10··O9	0.99(2)	2.63(2)	3.371(2)	131.4(19)
C5—H11··O9	0.96(3)	2.51(2)	3.396(2)	153.1(18)
C6—H13··O7	0.96(3)	2.49(3)	3.380(3)	154(3)

[a] Uncertainties, in parentheses, in units of the last digit. See Table S9 for details regarding other, less important short contacts.

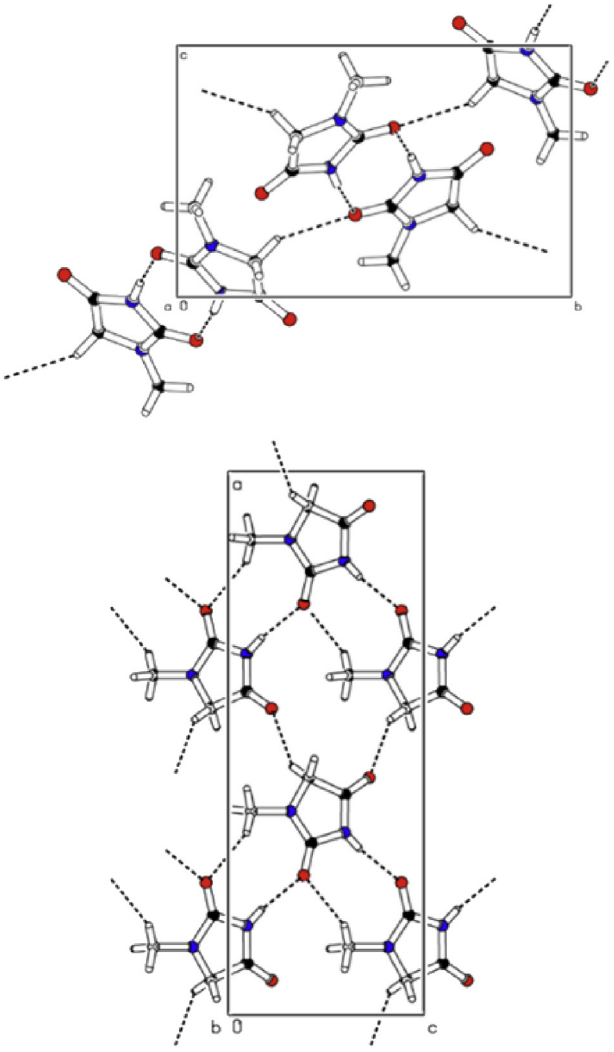

Fig. 1. Crystallographic unit cell of the two polymorphs of 1-MH. *Top*: polymorph I; *bottom*: polymorph II. Main contacts are indicated by the dashed lines. Atom color codes: white, hydrogen; black, carbon; red, oxygen; blue, nitrogen. (For interpretation of the references to colour in this figure legend, the reader is referred to the web version of this article.)

experiments, the laser power at the sample was approximately 15 mW, and the exposure time between 25 and 80 s. In the single crystal Raman measurements, a 100x objective lens was used, giving a laser spot diameter of 0.8 μm at the sample. Individual spectra were obtained with 1.5 cm^{-1} resolution. The final spectra were the mean of 50 scans for every sample.

In the temperature variation Raman studies, the sample was placed in a hot stage THMS 600 (Linkam Scientific Instruments) controlled by a T95-PE Linkpad controlling unit. The heating rate was set up at 10 °C min^{-1}. At each selected temperature, the Raman spectrum, in the 1000-1850 cm^{-1} range, was recorded, with a 30 s acquisition time and 20 accumulations.

2.3. X-ray crystallography

The single crystal X-ray measurements were carried out using a Bruker APEXII diffractometer, at 293(2) K, using graphite-monochromated MoKα (λ = 0.71073 Å) radiation. Data integration and scaling were performed with the SAINT suite of programs [11] and absorption corrections were done using SADABS [11]. The structure was solved by direct methods using SHELXT-2014/5 [12]. Refinements were carried out with the SHELXL-2016/6 package [13]. All refinements were made by full-matrix least-squares on F^2, with anisotropic displacement parameters for all non-hydrogen atoms (see Table S1 in the Supporting Information for details regarding the crystallographic analysis). All hydrogen atoms could be located on a difference Fourier synthesis; their positions were refined as riding on parent atoms with an isotropic temperature factor using SHELXL-2016/6 defaults [13]. Indexing of the crystal faces prior to single crystal Raman measurements was performed using the indexing procedure of the APEX2 software [11], based on the orientation matrix, from a set of video frames of the crystals mounted on the goniometer head. A CIF file containing supplementary crystallographic data was deposited at the Cambridge Crystallographic Data Centre with reference CCDC 1552440.

3. Results and discussion

3.1. Polymorphs screening and X-ray diffraction experiments

As mentioned in Section 2.1, the performed crystal screening involved recrystallization of 1-MH from a series of solvents. Two polymorphs were obtained: polymorph I, from dichloromethane, dioxane, water and ethanol solutions, and polymorph II from methanol solution. Recrystallization from acetone and tetrahydrofurane (THF) solutions gave rise to a mixture of both polymorphs, polymorph I being in general present as the major component.

The preliminary characterization of the samples was performed by differential scanning calorimetry (DSC; see Figure S1 in the Supporting Information), as described in our previous publication [9]. The DSC heating curves of the samples resulting in exclusive production of polymorph I show the melting peak at T_{fus} = 155.7 ± 0.7 °C, with an enthalpy of fusion $\Delta_{fus}H$ = 21.5 ± 0.3 kJ mol^{-1}, and no further events. In turn, that obtained from the sample recrystallized from methanol, exhibits a low energy solid-solid transition, extending from about 110 to 135 °C, corresponding to the conversion of polymorph II into polymorph I, which then melts at its expected temperature [9]. This latter DSC heating curve profile was also obtained in the case of the samples recrystallized from acetone and THF, but the Raman measurements demonstrated that in these two cases the original samples were a mixture of the two polymorphs, the relative amounts of each polymorph formed depending on the investigated sample (a trend was noticed for polymorph I to crystallize predominantly near the edges and polymorph II in the central surface of the crystallization vessel).

Crystals of the two polymorphs suitable for structure determination were collected from samples and investigated by single crystal X-ray diffraction. A summary of the most relevant crystallographic data for both polymorphs is presented in Tables 1 and 2.

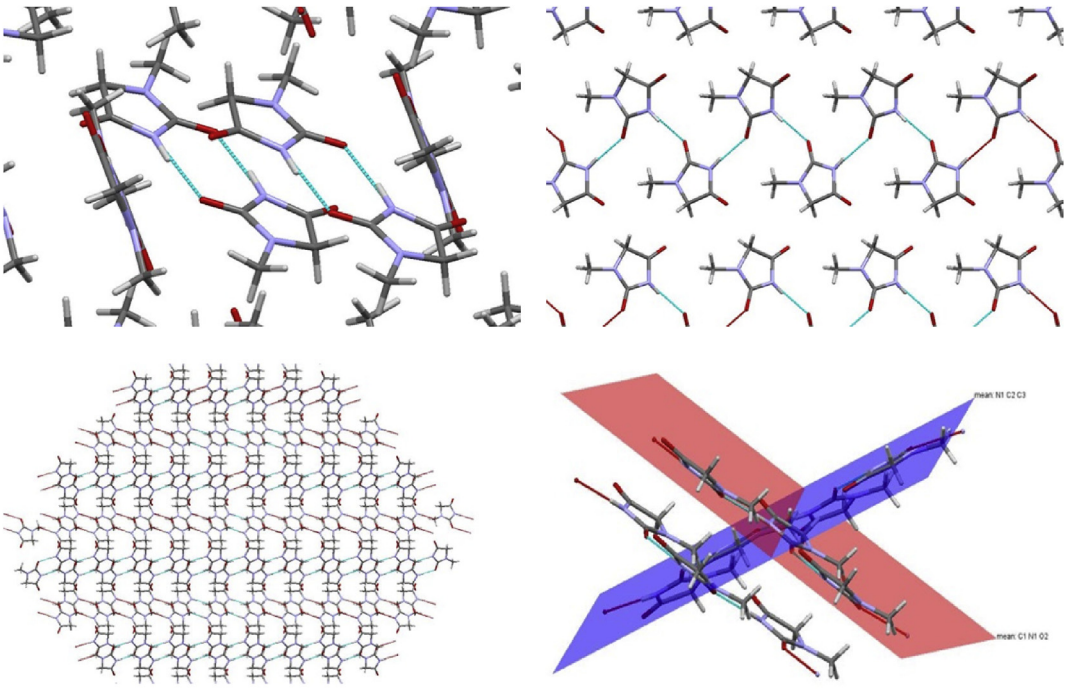

Fig. 2. Hydrogen-bonding schemes for the two polymorphs of 1-MH. *Left*: polymorph I; *right*: polymorph II. The N3—H8••O7 hydrogen bond shown in light blue. Atom color codes: white, hydrogen; black, carbon; red, oxygen; blue, nitrogen. (For interpretation of the references to colour in this figure legend, the reader is referred to the web version of this article.)

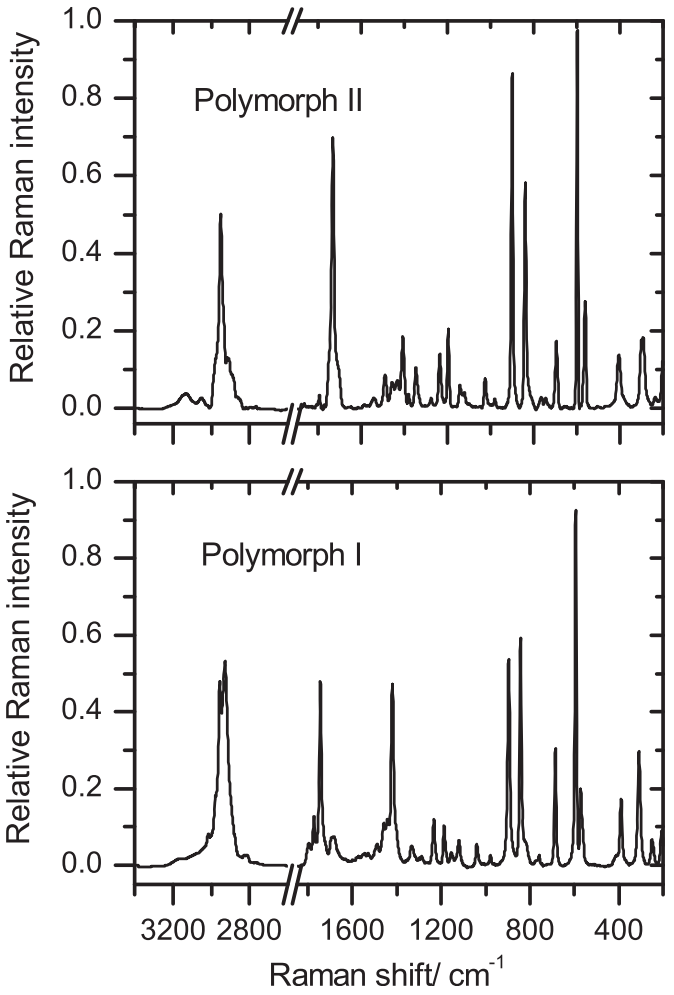

Fig. 3. 1-MH bulk Raman spectra (3300-400 cm^{-1} range) of 1-MH polymorphs. *top*: polymorph II; *bottom*: polymorph I.

The results obtained for the crystal of polymorph I replicated those previously reported in the literature [10]. The crystal is monoclinic, $P2_1/c$; $Z = 4$, $a = 5.601(10)$ Å, $b = 12.178(3)$ Å, $c = 8.090(2)$ Å, $\alpha = \gamma = 90°$ and $\beta = 105.62(2)°$. In the crystal, the hydantoin ring is essentially planar, with the C2=O7 bond length being longer than the C4=O9 one (1.2278(18) *vs.* 1.2110(18) Å). Though for the isolated 1-MH molecule the C=O bond lengths follow the same order, with the C2=O7 bond being slightly longer than the C4=O9 distance (1.210 *vs.* 1.207 Å; DFT/B3LYP/6-311++G(d,p) calculated data [9]), a result that has been discussed in detail in ref. 9, in the crystal of polymorph I the difference between these two bond lengths increases significantly. In particular, the C2=O7 bond length is considerably longer than for the isolated molecule. Such result can be explained considering that the O7 atom participates in the hydrogen bonding network in the crystal, whereas the O9 atom remains free (see Fig. 1 and Table 2). The most relevant pattern of hydrogen bonds noticeable in the crystal of polymorph I is the centrosymmetric ring formed by N3–H8···O7 interactions, which group 1-MH molecules in dimeric units (Fig. 1). The O7 atom takes part also in a non-conventional C5–H10···O7 interaction connecting 1-MH dimers together, resulting in a binary chain pattern. On the whole, intermolecular rings and chains give rise to an undulated pattern of hydrogen bonding (Fig. 2) that is mostly determined by the weak C5–H10···O7 interaction and the sp^3 hybridization of the C5 atom.

The new data obtained for polymorph II are provided in details in the Supporting Information (Tables S2–S9). Polymorph II is orthorhombic, $Pna2_1$ space group, with $Z = 4$, $a = 19.0258(4)$ Å, $b = 3.91210(10)$ Å and $c = 6.82880(10)$ Å. As in polymorph I, in this polymorph the hydantoin ring is also almost planar, and the C2=O7 bond is also longer than the C4=O9 distance (1.22105(20) *vs.* 1.21566(20) Å). However, in polymorph II the difference between the two C=O bond lengths is reduced to about 1/3 (0.0054 Å in polymorph II, compared to 0.0168 Å in polymorph I), because in the new polymorph the O9 atom participates in non-conventional C–H···O interactions with the two C5–H bonds (see Fig. 1). These interactions cause a slight elongation of the C4=O9 bond. In turn, the O7 atom participates, also as in polymorph I, in N3–H8···O7 interactions, but the C5–H10···O7 interaction (with the methylene ring group) existing in polymorph I is replaced in polymorph II by the slightly stronger C6–H13···O7 interaction (with the methyl substituent). The striking difference between the H-bond network in the two polymorphs is that, while in polymorph I the N3–H8···O7 interactions group the molecules in dimers (which are then associated by the C5–H10···O7 weak interactions), in polymorph II the N3–H8···O7 interaction is used to form zigzag chains, which are interspersed with other chains through the interactions involving O9 and form an angle of *ca.* 36° between them (see Figs. 1 and 2).

As it could be expected, the crystallographic data concerning H-bonding confirm our previous proposition [9] in relation to the relative strength of the H-bonds associated with the NH fragment in the two polymorphs, which has been extracted based on simple empirical correlations between the observed NH frequency shifts (for both the ν(NH) and γ(NH) modes) in going from the isolated molecule to the crystalline forms and the H-bond enthalpies [9,14,15]. The estimations obtained from the empirical correlations for the room temperature crystals suggested slightly stronger N–H bonds in polymorph I than in polymorph II [9]. The structural data shown in Table 2 is indeed fully consistent with the predictions regarding the relative strength of the H-bonds associated with the NH fragment in the two polymorphs (*i.e.*, the N3–H8 bond length is longer, while both N3···O7 and H8···O7 distances are shorter, and the H-bond angle is closer to linearity in polymorph I than in polymorph II).

3.2. Raman spectroscopy experiments

The Raman spectra of powdered samples of the two polymorphs are shown in Fig. 3, and clearly show different patterns. The proposed band assignments are given in Table 3, where they are compared with those previously given for the corresponding infrared spectra of the polymorphs and also for the IR spectra of the isolated 1-MH molecule in an argon matrix and calculated at the DFT(B3LYP)/6-311++G(d,p) level [9].

The major frequency shifts in going from the isolated molecule situation to the crystalline phases have been discussed in detail in our previous article [9] and occur for the ν(NH), δ(NH) and γ(NH) bands, which amount to *ca.* −530, +150 and +(270-300) cm^{-1} (average values), respectively, for the bands associated with the stretching vibration of the carbonyl group involved in H-bonding, ν(C4=O7), which shift by *ca.* −40 cm^{-1}, and for the bands assigned to ring stretching modes that, according to the previously reported normal mode analysis [9], have additional significant contributions from the δ(NH) coordinate (ν_4(ring) and ν_1(ring), which shift by *ca.* 20 and 40 cm^{-1}, respectively).

The most significant differences between the Raman spectra of the two polymorphs occur in the region below 950 cm^{-1}, where the two materials have bands appearing at clearly different frequencies (see Table 3), but the different spectroscopic signatures of the two

Table 3
Assignment of Raman spectra for polymorphs I and II of 1-MH. Comparison is made with the previously reported infrared (IR) data of the two polymorphs and of the isolated 1-MH in an argon matrix, as well as the DFT(B3LYP)/6-311++G(d,p) calculated spectra [9].

Experimental					Calculated (DFT(B3LYP)/g-311++G(d,p)) [9]			
Polymorph I		Polymorph II		Isolated molecule (Ar matrix; 10 K) [9]				Approximate description[e]
IR[a] [9]	Raman[a]	IR[a] [9]	Raman[a]	IR[a]	Freq[b]	I_{IR}[c]	I_{Raman}[d]	
3202/3142/3045/2819/2776/2744	3173/3075/30147 2827/2816/2759	3257/3192/3128/3072/3047/2752/2723	3200/3130/3089/3049/2976/2765	3488/3482	3486	85	108	ν(NH)
2983	2977	2984	2976	n.obs.	3076	1	41	$\nu(CH_3)$as.′
2957	2955	2952	2950	2962/2960	3004	21	61	$\nu(CH_3)$as.′′
2957	2955	2939	2937	2951	2995	21	126	$\nu(CH_2)$as.
2933	2928	2928	2916/2907	2930	2964	28	237	$\nu(CH_2)$s.
2886	2879	2886	2890/2882	2927/2883[e]	2956	55	137	$\nu(CH_3)$s.
1800/1770	1800/1795/1774/	1803/1770	1796	1805/1803	1804	174	36	ν(C4=O9)
1748/1727/1709/1688	1744/1723/1695/1684	1751/1728/1709/1687	1752/1733/1711/1704	1771/1768/~1753	1770	1053	4	ν(C2=O7)
1516	1529	1517	1542	1505/1492	1498	34	9	$\delta(CH_3)$as.′
1457	1458	1462	1459	1457/1455	1464	12	10	$\delta(CH_3)$as.′′
1452	1442	1456	1459	1456/1454	1461	52	8	$\delta(CH_2)$
1421	1420	1427	1434	1430/1427	1426	39	7	$\delta(CH_3)$s.
1417/1415	1420/1403	1414/1383	1408/1381	1413/1412/1407/1404/1401/1396	1406	124	9	ν_2(ring)
1500	1489	1489	1491	1343/1342/1337/1335	1331	45	2	δ(NH)′
1342	1333/1329	1343	1348	1319/1316	1303	138	2	ν_4(ring)
1289	1289/1288	1291/1280	1277	1295/1292	1278	14	1	ν(NC)
1236	1233	1240/1235	1237	1237/1235/1232	1233	35	5	$w(CH_2)$
1198/1191	1187	1198	1197	1180/1176	1178	4	3	$tw(CH_2)$
1125/1114	1133/1120	1125	1124	1131	1125	0.2	4	$\gamma(CH_3)$′′
1150/1145	1154	1145	1142	1121/1119/1116/1112/1108	1099	103	1	ν_1(ring)
1043	1040	1028	1027	1029/1028	1020	42	5	$\gamma(CH_3)$′
983	978	982	981	995/986	990	0.2	0.2	$\gamma(CH_2)$
898	895	901	901	884/883	873	15	9	ν_5(ring)
845	842	844/835	840	816	805	6	5	ν_3(ring)
754	795	745	745	752	739	12	0.3	γ(C2=O7)
701	686	700/687	696	688	680	7	4	δ_1(ring)
601	594	601	598	594/591/588/586/582	581	49	1	γ(C4=O9)
571	571	572	571		580	8	8	δ(C2=O7)
571	571	564	567	555/554	547	22	2	δ_2(ring)
817	821/795	771	766	530/527	526	77	1	γ(NH)
n.i.	389	n.i.	406	n.i.	377	22	2	δ(C4=O9)
n.i.	308	n.i.	300/292	n.i.	280	2	2	δ(NC)
n.i.	250	n.i.	237	n.i.	191	1	0.1	τ_1(ring)
n.i.	208	n.i.	202	n.i.	157	6	0.04	τ_2(ring)
n.i.	n.i.	n.i.	n.i.	n.i.	119	2	1	τCH_3
n.i.	n.i.	n.i.	n.i.	n.i.	79	0.4	0.2	γ(NC)

[a] Wavenumbers in cm^{-1}; n.obs., not observed; n.i., not investigated.
[b] Calculated frequencies scaled by 0.957 above 3400 cm^{-1} and by 0.980 below 3400 cm^{-1} [9].
[c] IR intensities in km mol^{-1}.
[d] Raman activities in $Å^4$ $a.m.u.^{-1}$.
[e] Assignments correspond to approximate descriptions of the vibrations chosen as the main coordinate contributing to the vibration (avoiding repetition) and are based on the PED's obtained for the isolated monomer [9]; abbreviations: w, wagging; tw, twisting; γ, rocking; ν, stretching; δ, bending; τ, torsion; s., symmetric; as., anti-symmetric; See Scheme 1 for atom numbering.

polymorphs extend to the whole spectrum. For example, the two most intense bands, at 1420 cm^{-1} ($\delta(CH_3)$ s.) and 1744 cm^{-1} (ν(C2=O7)) in polymorph I shift to 1434 and 1733 cm^{-1} in polymorph II. Also, the high frequency region, between 2700 and 3200 cm^{-1}, exhibits considerably dissimilar profiles in the two polymorphs (see Fig. 3). All these data suggest considerably different molecular arrangements in the two crystalline varieties, which is in agreement with the structural data obtained by X-ray diffraction.

The Raman spectra of single crystals of the two polymorphs are shown in Figs. 4 and 5. For polymorph I, the spectra were obtained with the laser excitation beam (direction X) perpendicular to the $(\bar{1}\ 02)$ face of the crystal and with the plane of polarization perpendicular (Y) and parallel (Z) to the $(\bar{12}\ 0)$ plane; for polymorph II, they were collected with the laser excitation beam (X) perpendicular to the (100) face of the crystal and with the plane of polarization perpendicular (Z) and parallel (Y) to the (001) plane (see Fig. 6 for images of the used crystals). In each case, spectra were collected with a polarizer selecting scattered light polarized perpendicularly or parallel to the plane of polarization of the excitation light, as well as without polarizer.

The detailed analysis of the spectra of the single crystals in what concerns the polarization effects is beyond the scope of the present article, requiring full treatment of the vibrations in the crystals space group framework. Essentially, one wants to show here that for both crystalline varieties polarization effects are rather relevant. For example, comparing the $X(YY)\bar{X}$ (parallel) spectrum of polymorph I with the $X(YZ)\bar{X}$ (perpendicular) spectrum, it can be observed that the bands at ~1420, 686, 594, 308 and 108 cm^{-1} [ascribed to ν_2(ring)/$\delta(CH_3)$ s, δ_1(ring), γ(C4=O9), δ(NC) and $\tau(CH_3)$] are considerably more intense in the first spectrum than in the second, while the bands at ~2935 (ν(NH)), ~1743 (ν(C4=O9)), 895

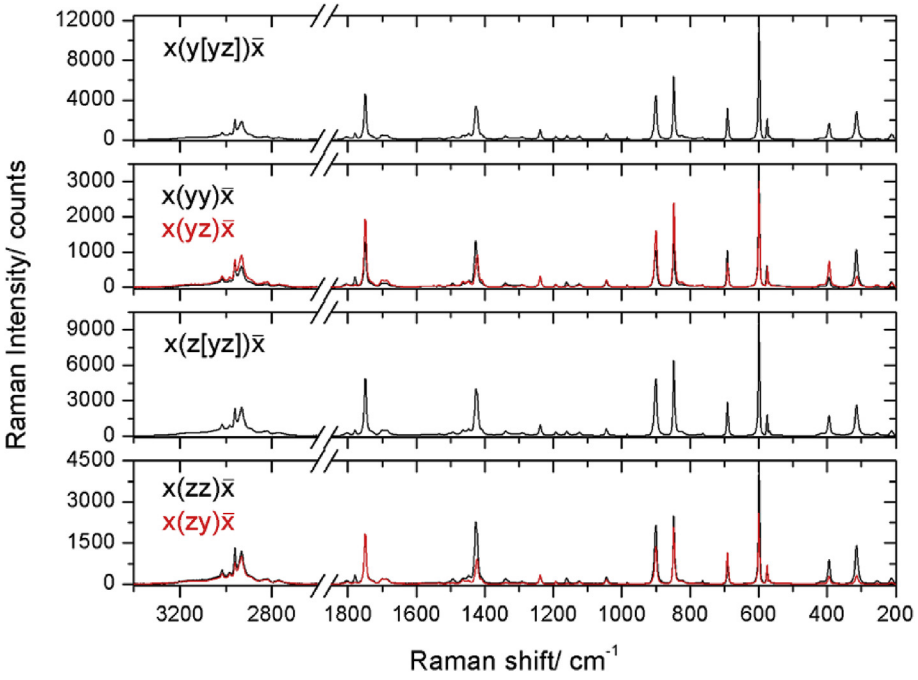

Fig. 4. Raman spectra of single crystals of polymorph I of 1-MH obtained on the crystal shown in Fig. 6.

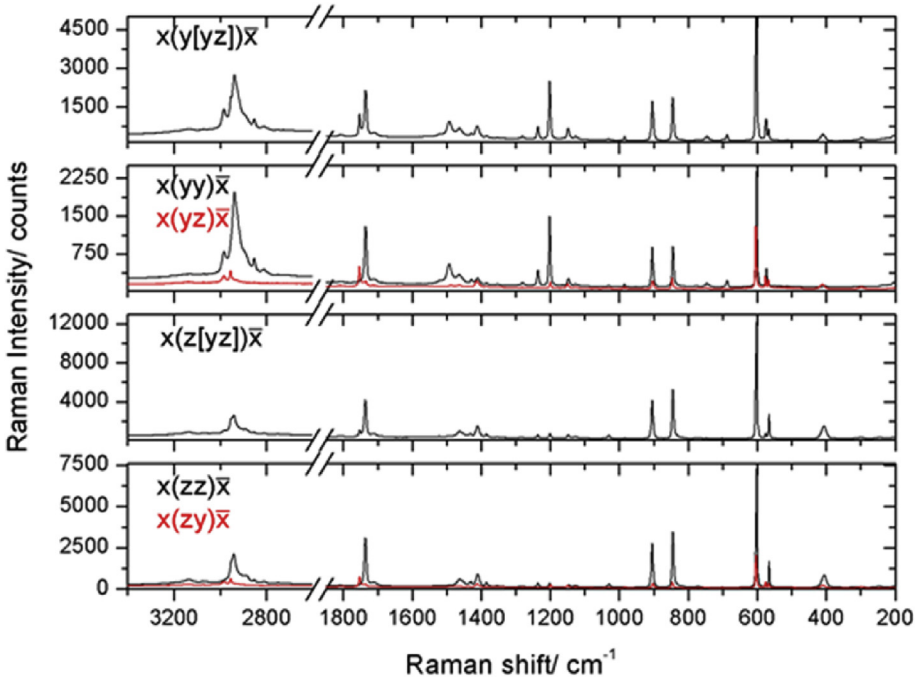

Fig. 5. Raman spectra of single crystals of polymorph II of 1-MH obtained on the crystal shown in Fig. 6.

(ν_5(ring)), 842 (ν_3(ring)) and 389 (δ(C4=O9)) cm^{-1} follow the inverse trend. The inverse trends are observed when comparing the X(ZZ)$\overline{X}$ spectrum with the X(ZY)$\overline{X}$ spectrum. For polymorph II the polarization effects are even more striking than for polymorph I, in particular in what concerns the relative intensities of different component-bands associated with the ν(NH) and ν(C=O) vibrations (see Fig. 5).

The phase transition between polymorph II and polymorph I was followed by single crystal Raman spectroscopy. The results are summarized in Fig. 7, which displays the temperature-dependent Raman spectra (in the 1000-1850 cm^{-1} spectral range) obtained for a sample of polymorph II submitted to heating ramp (at a rate of 10 °C min^{-1}) between 125 and 155 °C. The initial spectrum is identical to the X(Z[YZ])$\overline{X}$ spectrum of polymorph II shown in Fig. 5. Until T = 125 °C, no changes were observed in the spectrum. However, starting slightly above this temperature, the spectral profile changes noticeable and, at T = 145 °C, the spectrum is identical to that of polymorph I (specifically, it is practically coincident with the X(Y[YZ])$\overline{X}$ spectrum shown in Fig. 4). The range of temperature for the transformation was found considerably large

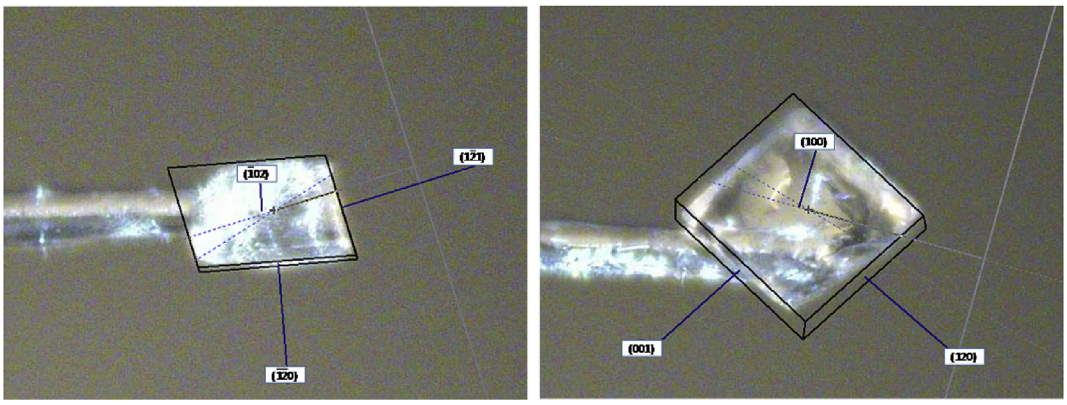

Fig. 6. Single crystals of polymorph I *(left)* and of polymorph II *(right)* of 1-MH used in the polarized Raman measurements. The Miller indices of the planes corresponding to the faces of the crystals are indicated in the figure; the laser beam (X direction) was focused on the upper faces of the crystals, and the spectra collected at 180° scattering geometry ($\overline{X}$); the crystals were sampled with the planes defining their side faces approximated aligned along the Y and Z directions (see text for details).

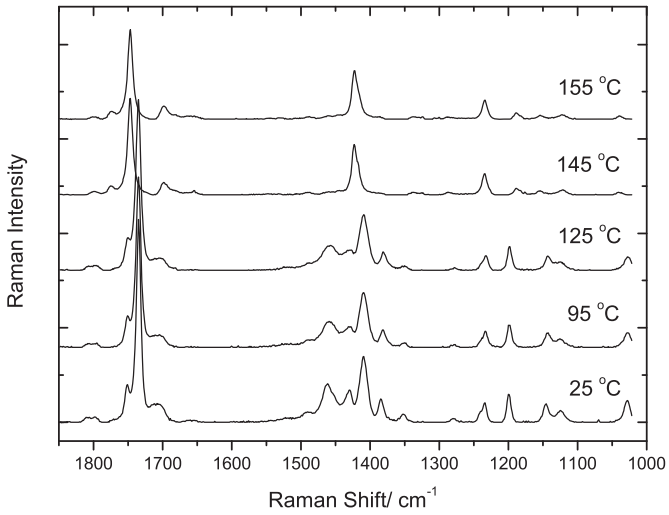

Fig. 7. Raman spectra of a single crystal of 1-MH (in the 1000-1850 cm^{-1} spectral region) showing the transformation of polymorph II into polymorph I, upon heating. Spectra are obtained without polarization analyzer, *i.e.*, for the reactant polymorph the spectrum corresponds to X(Z[YZ]$\overline{X}$) spectrum, shown in Fig. 5.

(~20 °C) in consonance with the previous data obtained by DSC and IR spectroscopy [9], and the fact that the temperature intervals in which the polymorph II to polymorph I transformation took place are slightly different in the different experiments (125–145 °C in the now reported Raman experiments, 95–155 °C as followed by IR for the compound in a KBr pellet, and 110–135 °C by DSC for the compound in an aluminum pan [9]) may be assigned to the dissimilar experimental conditions.

What is the most striking result achieved with the present single crystal Raman experiments is that they proved that the transformation between polymorph II and I, even though their structures are significantly distinct, is a non-destructive one, *i.e.*, the phase transition can take place without the initial crystal being destroyed to then reform the new one. Such information was not possible to obtain in both previously reported IR and DSC studies [9], which were performed for a macro bulk sample.

4. Conclusion

In this study, the polymorphism exhibited by 1-MH was investigated. After screening for polymorphs by recrystallization from different solvents, two polymorphs were identified, the first (polymorph I) corresponding to a known monoclinic ($P2_1/c$) crystalline variety whose structure had already been reported before [10], and the second (polymorph II) whose structure was determined for the first time in the present study. Polymorph II is orthorhombic, ($Pna2_1$), and exhibits a considerably different H-bond network, compared to polymorph I. Indeed, while in polymorph I the strongest N–H···O H-bond interactions group the molecules in dimers, which are then associated by weaker non-conventional C–H···O contacts, in polymorph II the N–H···O interaction originates zigzag chains of molecules, which are interspersed with other chains through weak C–H···O interactions involving O9 and forming an angle of *ca.* 36° with each other.

The two polymorphs were characterized in details by Raman spectroscopy, which was also used to follow the phase transition between them. Noteworthy, upon heating a single crystal of polymorph II, it converts into polymorph I (between 125 and 155 °C) in a non-destructive way, *i.e.*, the conversion taking place without the destruction of the original crystal. Such result constitutes also a new piece of information, which was not possible to obtain in both previously reported IR and DSC studies on 1-MH polymorphism [9], which were performed only for a macro bulk sample.

Acknowledgements

This investigation has been performed within the Project PTDC/QEQ-QFI/3284/2014 – POCI-01-0145-FEDER-016617, funded by the Portuguese *"Fundação para a Ciência e a Tecnologia"* (FCT) and FEDER/COMPETE 2020-EU. The Coimbra Chemistry Centre (CQC) is supported by FCT, through the project UI0313/QUI/2013, also co-funded by FEDER/COMPETE 2020-EU. CFisUC is funded by FCT through the project UID/FIS/04564/2016. Access to instruments from the TAIL-UC facility funded under QREN - Mais Centro project ICT_2009_02_012_1890 is gratefully acknowledged.

Appendix A. Supplementary data

Supplementary data related to this article can be found at http://dx.doi.org/10.1016/j.molstruc.2017.07.028.

References

[1] S.S. Block, Disinfection, Sterilization and Preservation, fourth ed., Lea & Febiger Inc., Philadelphia, USA, 2003.
[2] C.S.A. Kumar, C.V. Kavitha, K. Vinaya, S.B.B. Prasad, N.R. Thimmegowda, S. Chandrappa, S.C. Raghavan, K.S. Rangappa, Synthesis and *in vitro* cytotoxic

evaluation of novel diazaspiro bicyclo hydantoin derivatives in human leukemia cells: a SAR study, Investig. New Drugs 27 (2009) 327–337.
[3] C.V. Kavitha, M. Nambiar, C.S.A. Kumar, B. Choudhary, K. Muniyappa, K.S. Rangappa, S.C. Raghavan, Novel derivatives of spirohydantoin induce growth inhibition followed by apoptosis in leukemia cells, Biochem. Pharmacol. 77 (2009) 348–363.
[4] R. Sarges, R.C. Schnur, J.L. Belletire, M.J. Peterson, Spirohydantoin aldose reductase inhibitors, J. Med. Chem. 31 (1988) 230–243.
[5] K. Yang, Y. Tang, K.A. Iczkowski, Phenyl-methylene hydantoins alter CD44-specific ligand binding of benign and malignant prostate cells and suppress CD44 isoform expression, Am. J. Transl. Res. 2 (2010) 88–94.
[6] H.S. Park, H.J. Choi, H.S. Shin, S.K. Lee, M.S. Park, Synthesis and characterization of novel hydantoins as potential COX-2 inhibitors: 1,5-diarylhydantoins, Bull. Korean Chem. Soc. 28 (2007) 751–757.
[7] R.N. Comber, R.C. Reynolds, J.D. Friedrich, R.A. Manguikian, R.W. Buckheit, J.W. Truss, W.M. Shannon, J.A. Secrist, 5,5-Disubstituted hydantoins: syntheses and anti-HIV activity, J. Med. Chem. 35 (1992) 3567–3572.
[8] A.J. Cruz-Cabeza, C.H. Schwalbe, Observed and predicted hydrogen bond motifs in crystal structures of hydantoins, dihydrouracils and uracils, New J. Chem. 36 (2012) 1347–1354.
[9] B.A. Nogueira, G.O. Ildiz, J. Canotilho, M.E.S. Eusébio, R. Fausto, Molecular structure, infrared spectra, photochemistry, and thermal properties of 1-methylhydantoin, J. Phys. Chem. A 118 (2014) 5994–6008.
[10] M. Puszynska-Tuszkanow, M. Daszkiewicz, G. Maciejewska, Z. Staszak, J.B. Wietrzyk, B. Filip, M. Cieslak-Golonka, HSAB principle and nickel(II) ion reactivity towards 1-methyhydantoin, Polyhedron 30 (2011) 2016–2025.
[11] Bruker, APEX2, SAINT and SADABS, Bruker AXS Inc., Madison, Wisconsin, USA, 2014.
[12] G. Sheldrick, SHELXT - integrated space-group and crystal-structure determination, Acta Crystallogr. A 71 (2015) 3–8.
[13] G. Sheldrick, Crystal structure refinement with SHELXL, Acta Crystallogr. C 71 (2015) 3–8.
[14] M.S. Rozenberg, IR spectra and hydrogen bond energies of crystalline acid salts of carboxylic acids, Spectrochim. Acta A 52 (1996) 1559–1709.
[15] M.S. Rozenberg, G. Shoham, I. Reva, R. Fausto, Low temperature FTIR spectroscopy and hydrogen bonding in cytosine polycrystals, Spectrochim. Acta A 60 (2004) 463–470.